# INVESTIGATION OF SOLAR PRESSURE EFFECTS AT IRIDIUM MISSION ALTITUDE AND SOLAR SAILING MITIGATION TECHNIQUES

G. L. Dixon, W. H. Boyce III and R. W. Shepperd
Boeing Satellite Operations & Ground Systems, Leesburg, VA

## ABSTRACT

The Iridium constellation comprises 66 identical satellites, which have been maintained in near-polar, near-circular orbits at a mission altitude of 780 km since mid-1998. Maintaining these vehicles within strict geometrical constraints allows the network to provide users with voice, paging, data and fax services anywhere in the world at any time. While Iridium's primary purpose is commercial, the number and distribution of its satellites around the globe makes it a unique platform for the study of environmental factors and perturbative forces acting at the upper reaches of Low Earth Orbit. In fact, such study is sometimes carried out as an integral part of maintaining the constellation's integrity. In order to function as a network, Iridium satellites must each maintain a constant average period and therefore a constant average semi-major axis (SMA) at all times (control box).

Iridium satellites experiencing solar minimum (minimum drag) and high solar beta angle (β) experience solar sailing effects. In some cases, solar sailing is beneficial because it counteracts drag, minimizing orbit decay. But in other cases it causes problems in maintaining control box requirements.

The solar sailing seen with the Iridium constellation provides us with the opportunity to study its effects on satellites and to discuss techniques to counteract this phenomenon relating to control box maintenance. This paper will discuss the theory of solar sailing on satellites, observed events experienced by Iridium satellites at mission orbit and mitigation techniques to counteract these events.

## INTRODUCTION

The Iridium Satellite LLC (ISLLC) constellation provides global, point-to-point telephony service[1]. The constellation consists of 6 orbit planes, equally spaced in right ascension of the ascending node (RAAN), each with 11 satellites, equally spaced in mean argument of latitude ($f$). The nearly-circular orbits have an inclination of 86.4 degrees and mean SMA ($a$) of 7155.8 km. Though the constellation's purpose is commercial, the number and global distribution of satellites provide a unique platform to study the space environment and perturbative forces such as solar radiation pressure (SRP).

Each satellite's period and hence its mean SMA must be maintained within small tolerances because of the geometrical constraints on satellite crosslinks. However, non-conservative forces of atmospheric drag and SRP combine to change the SMA over time, and these effects must be continually monitored and countered. Thus updates to the estimates of each satellite's state vector and observed orbit decay rate (SMA lowering) are made throughout each day as a routine part of real-time operations. The impetus of these updates is to develop an off-line capability to improve modeling of secular perturbations, thus improving prediction reliability and increasing the robustness of the products generated by the orbit analysis organization.

The overall observed orbit decay rate ( $\dot{a}_{Observed}$ ), comprises terms due to atmospheric drag, SRP, formation-keeping (FK) burns and smaller terms arising from Earth's albedo and Sun/Moon perturbations. At this altitude, and with the precision required, we comfortably ignore the smaller terms and write:

$$\dot{a}_{Observed} = \dot{a}_{Drag} + \dot{a}_{SRP} + \dot{a}_{FK} \qquad (1)$$

Data of observed orbit decay rate has been collected on the Iridium satellite constellation since start of service in 1998. It will be shown that during times of low drag and high solar beta angle (β) (angle between orbit plane normal vector and Sun vector shown in Figure 1), solar sailing effects have been witnessed on Iridium satellites.

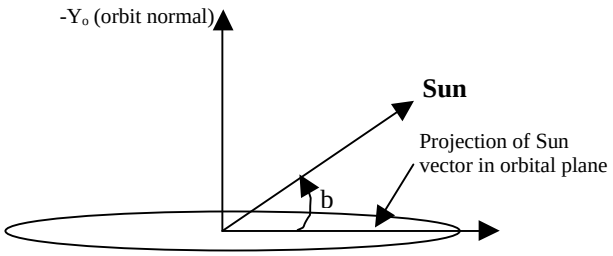


Figure 1: Geometry of orbit and Solar Beta Angle[8]

This paper will focus on an investigation of $\dot{a}_{SRP}$ and its effects on Iridium satellites at mission altitude. First will be a geometrical description of the Iridium satellite. Next, will be an explanation of data collection and interpretation. Finally, there will be a discussion of the SRP model used for the Iridium satellite, the extraction of observed SRP data, a comparison of the observed data to the model, and mitigating techniques used to counter SRP effects.

## IRIDIUM SATELLITE

### Geometry

The Iridium satellite, depicted in Figure 2, is composed of three subsections: the structural subsystem (SS), the main mission antenna panels (MMA) and the solar arrays (SA). The structural subsystem is a right triangular prism 10 feet long and thirty inches along each side. The 3 MMAs are 6 feet long and 30 inches wide, extending along the bottom edges of the SS. The two solar arrays are 11 feet long and 4 feet wide each, and extend from gimbals at the top of the SS.

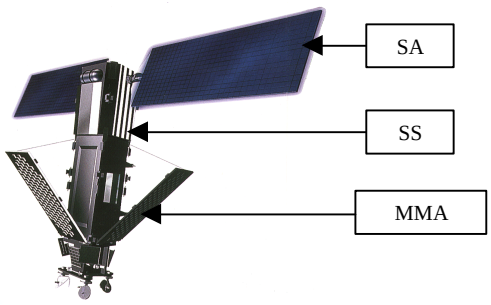


Figure 2: Iridium Satellite

### Satellite Coordinate System

The Iridium satellites are gravity gradient stabilized with solar array Sun tracking, *i.e.* the SS and the MMAs are always directed toward the nadir (+Z direction), while the solar arrays generally track the Sun. The +X direction of the coordinate system coincides with the nominal velocity vector of the satellite while the +Y direction makes up the right-handed system (Figure 3).

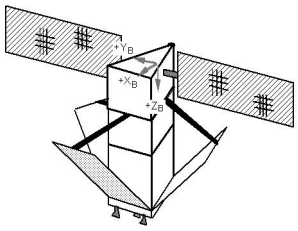


Figure 3: Iridium Satellite Coordinate System

Operationally the Iridium satellite only fires thrusters in the direction of the velocity vector. If thruster fire is needed in another direction the vehicle must perform attitude maneuvers to change orientation.

**Solar Array Configuration**

There are two primary solar array configurations for the Iridium satellite, forward (FWD) and forward low drag (FLD). The forward solar array configuration for the Iridium satellite was designed to be the nominal configuration for all iridium satellites, but due to solar sailing effects this configuration had to be modified. During low solar beta angles (absolute value), the satellite configurations are identical. The difference between the two configurations occurs at high solar beta angles where the solar arrays are locked but are in opposite directions relative to the velocity vector of the satellite.

*Forward Configuration*

In the forward configuration, shown in Figure 4, the X component of the normal vector of the solar arrays points in the -X direction or opposite the velocity vector. In this configuration the effects of SRP causes orbit raising, counter acting orbital decay.

*Forward Low Drag Configuration*

In the forward low drag configuration, shown in Figure 5, the X component of the normal vector of the solar arrays point in the +X direction or in the same direction of the velocity vector. In this configuration the effects of SRP causes orbit lowering, adding to orbital decay.

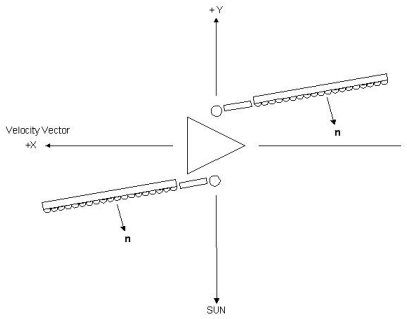


Figure 4: Iridium Satellite in Forward Configuration

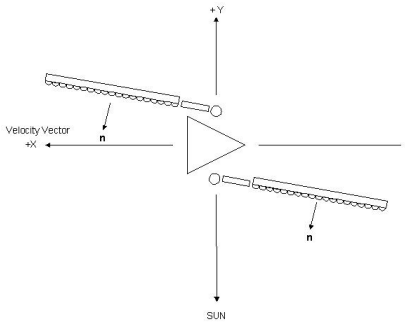


Figure 5: Iridium Satellite in Forward Low Drag Configuration

**COLLECTION OF DATA**

Maintenance of the control box for the Iridium satellite is an integral part of daily operations for the system. In order to maintain the control box, an up to date estimation of the position (SMA and $f$) must be obtained. Orbit estimation for the satellites is based on antenna angles and differential time of arrival measurements from ground stations. On each real-time pass, an extended Kalman filter processes this data along with a priori information about the orbit state, covariance matrix, current solar data (F10.7 and Ap) and a ballistic coefficient.

The orbit filter uses the Jacchia-Roberts[2,3] atmosphere model to determine an estimated atmospheric density $r$. It does not model SRP as an independent force, however; the combination of the force due to drag and SRP is assumed to be a "drag-like" force, proportional to the velocity squared ($v^2$) and in the negative tangential direction (unit vector given by $\hat{i}_t$), so that the two together are described by the usual drag equation.

$$\vec{F}_{Drag+SRP} = -Brv^2\hat{i}_t \qquad (2)$$

but ballistic coefficient, *B*, derived empirically from real orbit decay rate data rather than analytically from the vehicle's physical characteristics. The changes due to SRP are thus incorporated into the value of *B*.

For purposes of everyday operations, the estimation process was designed to yield an SMA accuracy in the 1-10 meter range and a $f$ accuracy in the tens of meters.

Each day individual SMA and ϕ measurements are taken from the previous 2, 3 or 4 days, depending on the best-fit sigma obtained. The $\dot{a}$ is found from both a linear fit to the SMA points and a quadratic fit to the $f$ points. This observed data is then corrected for formation keeping (FK) burns. These corrected SMA and $f$ measurements are trended to give an estimate of the orbit decay rate at epoch. A weighted average of these two terms is then done to obtain a final decay rate.

$$\dot{a}_{Corrected\_SMA} = \dot{a}_{Observed\_SMA} - \dot{a}_{FK} \qquad (3)$$

$$\dot{a}_{Corrected\_f} = \dot{a}_{Observed\_f} - \dot{a}_{FK} \qquad (4)$$

$$\dot{a}_{Corrected} = \frac{f_{SMA}\dot{a}_{Corected\_SMA} + wf_f\dot{a}_{Corrected\_f}}{f_{SMA} + wf_f} \qquad (5)$$

where

- ω - Absolute weighting factor
- $f_{SMA}$ - Weighting factor for SMA
- $f_f$ - Weighting factor for $f$

In terms of Equation 1, these points represent the combined effects of drag and SRP over the interval.

$$\dot{a}_{Corrected} = \dot{a}_{Drag} + \dot{a}_{SRP} \qquad (6)$$

The flexibility of the fit span helps mitigate the effects of transitory variations in solar activity during the days previous to the date of the measurement. Figure 6 shows a typical four-day fit, both observed and corrected.

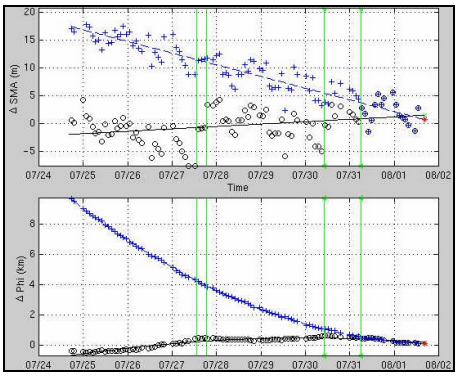


Figure 6: The solid line represents a fit without thruster firings; the dashed line "Burn Corrected Fit" accommodates the burns relative to the last estimation point.

Under the assumption that vehicles in a given orbit plane with the same solar array configuration will experience nearly identical drag and radiation environments, the individual $\dot{a}$ 's for each plane and for each solar array configuration are averaged. In a permanent file for later trending, the average $\dot{a}$ s for similarly configured satellites are entered for all six planes, along with the corresponding solar beta angles. A constellation-wide average is also calculated for $\dot{a}_{Corrected}$ . As shown in Figure 7, this gives a good average orbit decay as a function of time. The data used in this study covers the period starting beginning-1999 through the June of 2003.

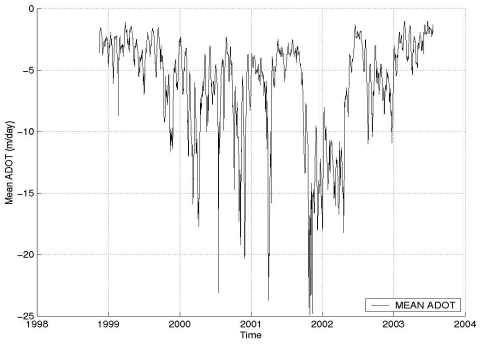


Figure 7: Constellation-wide average corrected orbit decay rate as a function of time.

## SOLAR RADIATION PRESSURE EFFECTS

### Solar Radiation Pressure Theory

The idea that solar sails could be used to effectively propel a space vehicle has been highly debated due to the conflicting thermodynamic rule presented by N.L. Sadi Carnot in 1824 and the electromagnetic rule presented by James Maxwell in 1871[9,10]. Carnot explained that radiation pressure exerted by incoherent light on surfaces was a thermodynamic process (heat engine) and that only a certain efficiency of kinetic energy could be obtained, zero efficiency if a perfect mirror was used because there would be no heat transfer to the mirror. While Maxwell explained that radiation pressure exerted by incoherent light on surfaces was an electromagnetic process. Contradictory to Carnot, if a perfect mirror is used the solar pressure obtained is twice the force exerted, due to the momentum change given by a surface with perfect reflectivity.

Both rules have valid points, but for this study the rules of Maxwell will be applied to investigate SRP data obtained from the Iridium constellation.

From Maxwell's equations we have the rate of energy flow defined as:

$$\vec{S} = \frac{1}{m_0}\vec{\mathrm{E}} \times \vec{B} \qquad (7)$$

$$\frac{dU}{dt} = SA \qquad (8)$$

where

- U - Energy
- S - Solar Intensity (Poynting Vector)
- A - Surface Area

Using Einstein's law relating energy and mass we have the momentum being:

$$U = E = mc^2 \qquad (9)$$

$$p = mc = \frac{U}{c} \qquad (10)$$

where

- p - momentum
- m - Mass
- c - Speed of Light

From the momentum we have the force being:

$$F = \frac{dp}{dt} = \frac{dU}{dt}\frac{1}{c} = \frac{SA}{c} \qquad (11)$$

Substituting the solar constant $\Phi_0$ for the intensity S, using the correct unit vector for the Sun (negative unit vector) and the surface area, and taking into account solar reflectivity we obtain a force equation of:

$$\vec{F} = \frac{-\Phi_0 A}{c}\left[(1-r)\vec{s} + 2\left(\frac{d}{3} + r\cos g\right)\vec{n}\right]\left|\cos g\right| \qquad (12)$$

where

- F - Force
- $r$ - Specular reflectivity
- $d$ - Diffuse reflectivity of elementary surface j
- $s$ - Unit vector in direction of Sun
- $n$ - Unit vector normal to $A$
- $g$ - Angle between $s$ and $n$

**Solar Radiation Pressure Model**

The analytical separation of the orbit decay rates into their drag and SRP components is accomplished by creating a simple multiple plate model of the satellite and calculating from it the $\dot{a}$ due to SRP[4]. Then SRP is defined as:

$$\dot{a}_{SRP} = \dot{a}_{Corrected} - \dot{a}_{Drag} \qquad (13)$$

The satellite is modeled as an assemblage of 10 flat plates with 15 surface elements as shown in Figure 8.

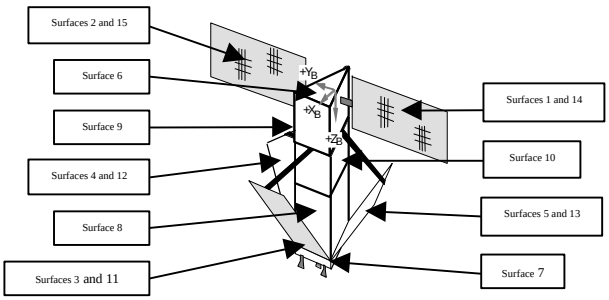


Figure 8: Satellite Plate Concept

The SS is modeled as 3 flat plates and 2 triangular flat plates on the top and bottom of the SS. Each of the 3 MMAs is modeled as a flat plate extending along the bottom edges of the SS. Each of the 2 solar arrays is represented as a flat plate extending from gimbals at the top of the SS.

The elementary force for each surface element at any given time is computed for a specified relative position of the satellite with respect to the Sun. For a flat plate the elementary force[5] acting on its surface is

$$\vec{F}_j = \frac{-\Phi_0 A_j}{c}\left[(1-r_j)\vec{s} + 2\left(\frac{d_j}{3} + r_j \cos g_j\right)\vec{n}_j\right]\left|\cos g_j\right| \quad (14)$$

where

- $F_j$ - Elementary force acting on surface j
- $A_j$ - Area of elementary surface j
- $r_j$ - Specular reflectivity of elementary surface j
- $d_j$ - Diffuse reflectivity of elementary surface j
- $n_j$ - Unit vector normal to $A_j$
- $g_j$ - Angle between *s* and $n_j$

If the Sun is not visible to the surface, the elemental force is naturally assumed zero. If the Sun is visible to the surface, the elemental force vector is computed.

The total SRP force acting on the satellite is found by summing the forces acting on each of the 15 surfaces. Since the mass of the vehicle is known, the acceleration in the direction of the velocity vector (+X) due to SRP ($acc_x$) is easily found. Then Gauss' form of the Legendre Planetary Equations[6] is invoked to calculate the rate of change of the semi-major axis:

$$\dot{a}_{SRP} = \frac{2a^2 v}{m} acc_X$$

$$\dot{a}_{SRP} = -\frac{2a^2\Phi_0}{mMc}\sum_{j=1}^{15} A_j\left[(1-r_j)\vec{s}\cdot\vec{v} + 2\left(\frac{d_j}{3} + r_j \cos g_j\right)\vec{n}_j\cdot\vec{v}\right]\left|\cos g_j\right| \quad (15)$$

where

- $\dot{a}_{SRP}$ - Time rate of change in semi-major axis for SRP
- $a$ - Semi-major axis
- $v$ - Velocity of satellite
- $M$ - Mass of satellite
- $m$ - Earth's gravitational constant

**Analysis of Data**

An algorithm incorporating the SRP model was written and run for the periods starting in early 1999 to the end of 2003. This was done to show changes in $\dot{a}$ (adot) over time[7].

*Prominence of SRP during low drag periods*

Figure 9 shows the relative magnitudes of $\dot{a}_{SRP}$ vs. $\dot{a}_{Corrected}$. During the low periods of the solar cycle, SRP has a greater relative influence on the $\dot{a}_{Corrected}$ of the satellites. This can be seen clearly during the period before mid-1999, the period during mid-2001 and the period during late-2002 when solar activity was low. Under such conditions, SRP counteracted drag and even produced solar sailing effects as shown in Figure 10. During the period depicted, the Kalman filter controls were widened to allow the un-modeled acceleration controls to account for the

change in semi-major axis from the un-modeled solar radiation pressure. The standard controls at the beginning and end of the period were not able to account for the effect until the atmospheric density increased enough to allow the filter to model the semi-major axis behavior.

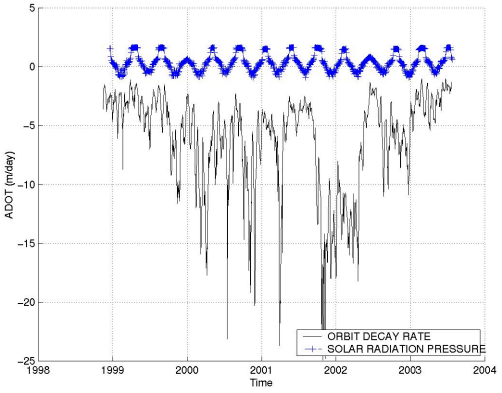


Figure 9: $\dot{a}_{Corrected}$ and $\dot{a}_{SRP}$ vs. Time

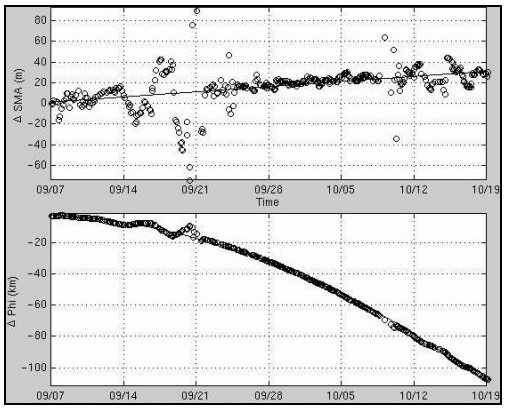


Figure 10: Solar sailing effect seen during a period of extremely low atmospheric drag The semi-major axes of the affected satellites increased approximately 40 meters over 40 days.

Also shown in Figure 9, it is clear that during this time span the $\dot{a}_{SRP}$ is cyclical compared to the wide range of $\dot{a}_{Corrected}$. Since the SRP is proportional to $\Phi_0$, the reason for the cyclical nature is that the solar arrays track the Sun as the solar beta angle progresses. This makes the $\dot{a}_{SRP}$ mainly a function of the beta angle. As mentioned earlier, the constellation has six planes that rotate through all beta angles. Figure 11 shows this cycle. The relative value of $\dot{a}_{SRP}$ generally increases with increasing absolute value of β.

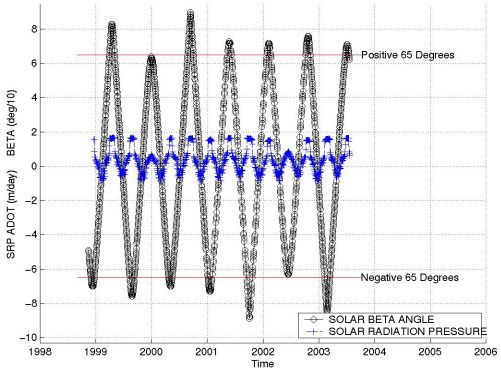


Figure 11: $\dot{a}_{SRP}$ and Sun β Angle vs. Time for Plane 6

*Investigation of different solar array configurations*

As mentioned before there are two primary solar array configurations for the Iridium satellite, forward (FWD) and forward low drag (FLD). Theses different configurations provide us with a unique analytical opportunity because during higher absolute solar beta angles the satellites are configured in opposite directions relative to the velocity vector of the satellite. The SRP experienced by the FWD configured satellites has an orbit raising effect, counteracting orbit decay, while the SRP experienced by the FLD configured satellites has an orbit lowering effect, adding to orbit decay. Looking at the data, when the absolute value of 65 degrees in beta is reached, the adot due to SRP values for both configurations go in opposite directions (Figures 12 a,c,e). Thus, the total decay rate (From SRP

and Drag) experienced by the FWD vehicle has higher values of adot compared to the FLD vehicle (Figures 12 b,d,f).

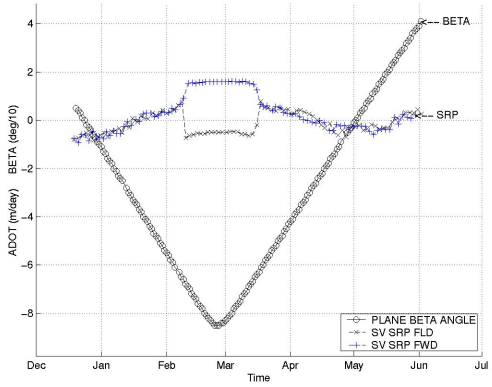


Figure 12(a): Plane 1 – SRP adot and beta angle vs. time.

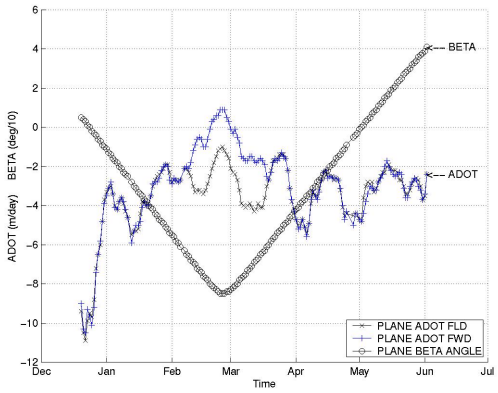


Figure 12(b): Plane 1 - Total adot (SRP and Drag) and beta angle vs. time.

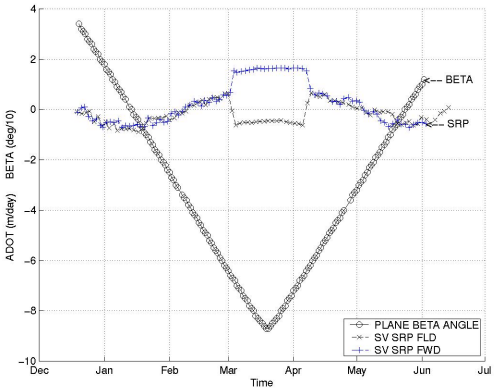


Figure 12(c): Plane 2 – SRP adot and beta angle vs. time.

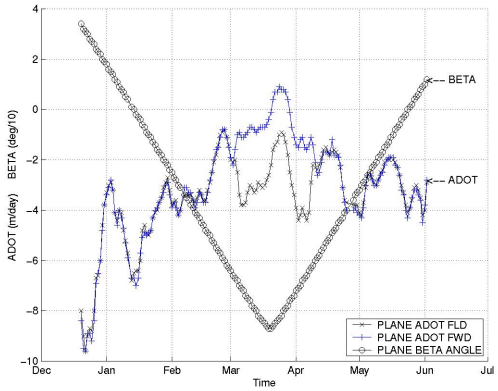


Figure 12(d): Plane 2 - Total adot (SRP and Drag) and beta angle vs. time.

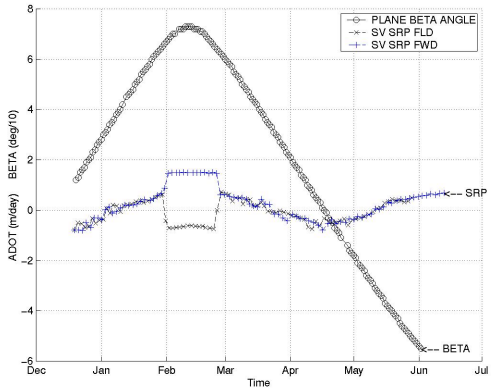


Figure 12(e): Plane 6 – SRP adot and beta angle vs. time.

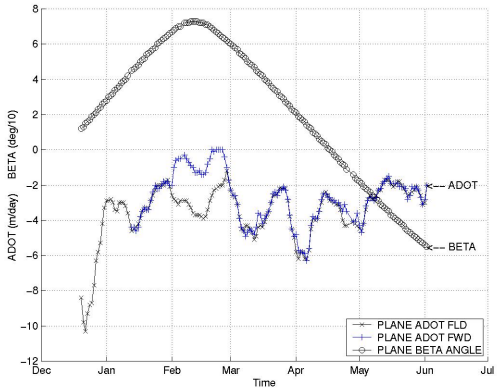


Figure 12(f): Plane 6 - Total adot (SRP and Drag) and beta angle vs. time.

Taking the difference in adot of the modeled SRP for the FWD and FLD configured vehicles and comparing it with the difference in adot of the corrected total adot due to SRP and drag (Equation 6) for the FWD and FLD configured

vehicles, we see interesting results. The modeled difference coincides with corrected data. This can be seen in Figure 13.

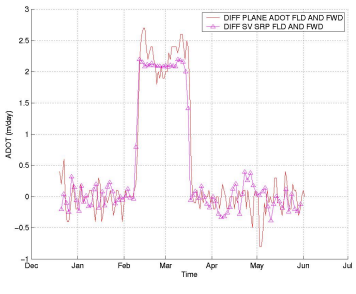


Figure 13(a): Plane 1 – Modeled difference in SRP adot compared with observed difference in total adot (SRP and Drag)

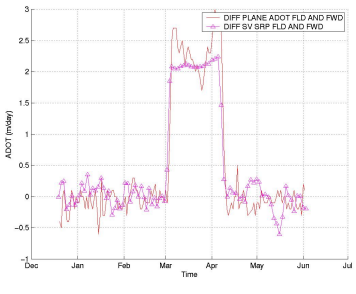


Figure 13(b): Plane 2 – Modeled difference in SRP adot compared with observed difference in total adot (SRP and Drag)

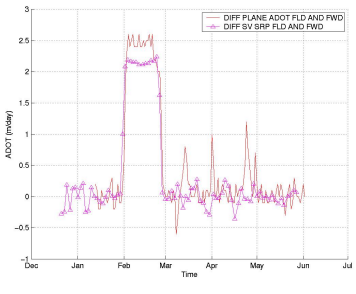


Figure 13(c): Plane 6 – Modeled difference in SRP adot compared with observed difference in total adot (SRP and Drag)

Looking at the data there is a slight difference in the corrected adot data and the SRP data. This difference comes from the fact that the FLD configuration has a slightly greater profile than the FWD configuration ($2*A_{SA}*\sin(10^{o})$), where $A_{SA}$ is the surface area of a solar area. This will give a slightly greater drag value for FLD. A variable D, which is a function of F10.7 Solar Flux, will represent the difference in drag.

$$\Delta\dot{a}_{Corrected} = \Delta\dot{a}_{Drag} + \Delta\dot{a}_{SRP} \qquad (16)$$

$$\Delta\dot{a}_{Drag} \cong D(F10.7) \qquad (17)$$

$$\Delta\dot{a}_{Corrected} \cong \Delta\dot{a}_{SRP} + D(F10.7) \qquad (18)$$

Figure 14 shows the relationship of this difference:

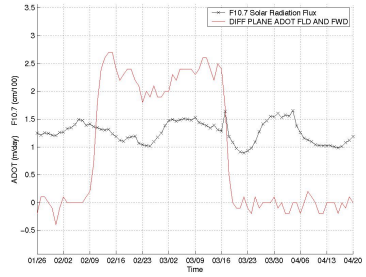


Figure 14(a): Plane 1 - Relationship of $\Delta\dot{a}_{Corrected}$ and F10.7 Solar Flux

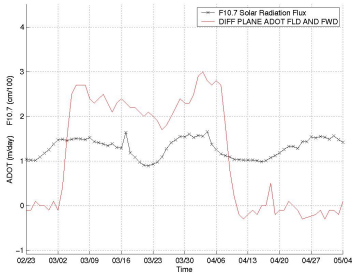


Figure 14(b): Plane 2 - Relationship of $\Delta\dot{a}_{Corrected}$ and F10.7 Solar Flux

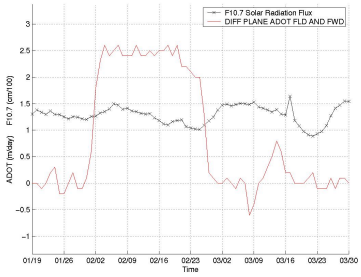


Figure 14(c): Plane 6 - Relationship of $\Delta\dot{a}_{Corrected}$ and F10.7 Solar Flux

The remaining difference in the term of SRP agrees both in the model and in corrected data.

$$\Delta\dot{a}_{SRP} \cong \Delta\dot{a}_{Corrected} - D(F10.7) \qquad (19)$$

*Errors, Impacts and Future Study*

Though the data correlates well the amplitude of the data is a function of optical properties for the individual plates of the satellite. Known coefficients can be obtained, but due to environmental effects experienced over time there is no guarantee that these coefficients reflect the current properties of the satellite. Further study can be done to find the time degraded solar reflectivity coefficient values for the satellites.

From the observed data, the difference in total adot for the FWD and FLD configured vehicles was obtained. This was done to cancel out adot due to drag and to show the difference in SRP for both solar array configurations. The difference due to drag for total adot is small but significant. Further study can be done to correct for this difference and obtain observed data with just adot due to SRP.

**Solar Sailing Mitigation for Control Box Maintenance**

With the onset of low drag and high solar beta angles, the perturbative force of SRP becomes a major variable in control box maintenance. To mitigate these effects different techniques can be used.

The control box for the Iridium satellite has a Y axis representing the SMA and an X axis representing $\phi$.

The equation that defines the associated parabolic path flight is:

$$\Delta f = -\frac{3p}{2aP\dot{a}}\Delta a^2 \qquad (20)$$

where

- $\Delta a$ - Semi-major axis measured from the center of the control box
- $\Delta f$ - Mean argument of latitude measured from the center of the control box
- $P$ - Period of Orbit
- $a$ - Absolute semi-major axis

Under normal operating conditions, the value of $\dot{a}$ is negative. Looking at Equation 20 this causes a parabolic flight path displayed in Figure 15 (a). This is the nominal flight path of the Iridium satellites. When SRP is prevalent it creates a positive value in $\dot{a}$, which causes a parabolic flight path displayed in Figure 15 (b). This flight path leads to orbit raising.

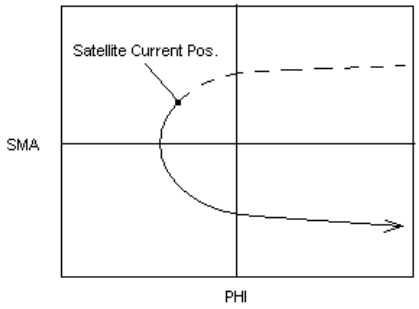


Figure 15(a): Control box for Iridium satellite and flight path during normal operations.

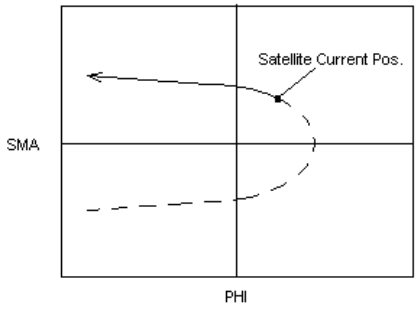


Figure 15(b): Control box for Iridium satellite and flight path during high beta low drag periods.

There are several techniques that can alleviate this problem and they are as follows:

- Retrograde thruster firing
- Increase drag profile on satellite
- Avoid upper quadrants of control box during high beta low drag periods

Firing in the direction against the velocity vector will give $\Delta V$ to lower the satellites orbit. Appendages on the satellite, such as the solar arrays, can be modified to give a larger drag profile to lower the satellites orbit. Also, The position of the satellite can be placed in the lower quadrants of the control box to extend time of cycle through high beta periods.

## CONCLUSION

A geometric plate model was used in the creation of an algorithm to calculate adot due to SRP. This algorithm was then run for two different solar array configured satellites (FWD and FLD) where their difference in $\dot{a}_{SRP}$ was recorded. This data was then compared with data of observed differences in total adot for these two configurations. It can be seen from the data that the observed (after weighted correction of SMA and $\phi$) difference in $\dot{a}_{Corrected}$ for the FWD and FLD configured satellites correlate to the modeled differences of $\dot{a}_{SRP}$ . Knowing that the modeled differences are based on Maxwell's equations it can be shown that these equations apply for satellites at the Iridium mission altitude of 780 km.

The authors would like to express their thanks to the many people at Boeing Corp. and Iridium Satellite LLC who made possible the generation, collection and presentation of the data contained herein.

## REFERENCES

1. Puderbaugh, A. L., Dixon Jr., G. L., Shroyer, L. E., Boyce III, W. H., *A Global and Local History of Drag Effects at Iridium Mission Altitude, 2002.*

2. Jacchia, L.G, "New Static Models of the Thermosphere and Exosphere with Empirical Temperature Profiles," *Smithsonian Astrophysical Observatory (SAO) Special Report 313*, May 1970.

3. Roberts Jr., Charles E., "An Analytical Model for Upper Atmosphere Densities Based Upon Jacchia's 1970 Models," *Celestial Mechanics*, 1971.

4. Kubo-oka, Toshiro and Arata Sengoku, "Solar radiation pressure model for the relay satellite of SELENE," *Earth Planets Space*, 51, 1999.

5. Milani, A., A.M. Nobili, and P. Farinella, *Non-gravitational Perturbations and Satellite Geodesy*, Universita di Pisa, Italy, 1987.

6. Battin, Richard H., *An Introduction to the Mathematics and Methods of Astrodynamics*, AIAA Education Series, 1987.

7. Vallado, David A., *Fundamentals of Astrodynamics and Applications*, Space Technology Series, 1997.

8. Team 4, Stanford CubSat Project, Stanford University, 2001.

9. Parsons, Paul, *Solar sailing 'breaks laws of physics'*, New Scientists, 2003.

10. Benjamin Diedrich, *Letter to the Editors of New Scientist Re: Solar Sailing Breaks Laws of Physics, New Scientists, 2003.*